Charged pion photoproduction with the Δ(1232) baryon beyond the resonance region

Seung-il Nam[*] and Byung-Geel Yu[†]

Research Institute for Basic Sciences, Korea Aerospace University, Goyang 412-791, Korea
(Received 10 May 2011; revised manuscript received 5 July 2011; published 18 August 2011)

We investigate the charged pion photoproduction off the proton target with the $\Delta(1232)$ baryon, i.e., $\gamma p \to \pi^- \Delta^{++}(1232)$ and $\gamma p \to \pi^+ \Delta^0(1232)$, based on the effective Lagrangian method, beyond the resonance region, $\sqrt{s} \gtrsim 2$ GeV. We employ the π- and ρ-meson Regge trajectories in the t channel, in addition to the proton and Δ pole, in the s and u channels, respectively, and the contact-interaction contributions. A specific scheme for the form factor which satisfies the Ward-Takahashi identity, crossing symmetry, and on-shell condition is taken into account. We also consider a smooth interpolation between the Regge and Feynman propagators for the t-channel meson exchanges as a function of the Mandelstam variable s. We present the numerical results for the energy and angular dependences of the cross sections and the double- and single-polarization observables. It turns out that the present framework reproduces the experimental data qualitatively very well. In particular, the interpolation between the two propagators plays a crucial role in reproducing the high-energy experimental data correctly. The π^+ decay-angle distribution is also studied using the Δ^{++}-decay frame, i.e., the Gottfried-Jackson frame. The present results will be a useful guide for future high-energy photon-beam experiments.

I. INTRODUCTION

Hadron productions via various scattering processes have been one of the most important experimental and theoretical methods to investigate the strongly interacting systems, which are governed by the fundamental theory, i.e., quantum chromodynamics (QCD), in terms of the color-singlet degrees of freedom. Among the various production processes, photo- and electroproduction have proved to be very useful [1–3]. Since the photon is a clear probe, these production processes are well suited for investigating hadronic properties, such as the structures, reaction mechanisms, and so on. Moreover, the non-strange-meson electro- and photoproduction are extremely good methods to investigate the nucleon-resonance search. On top of these specific features, according to a gauge boson by nature, coupling of the photon constrains the scattering processes in such a way that the Ward-Takahashi (WT) identity must be satisfied to all orders of Feynman diagrams. Due to this constraint, one can identify simply the necessary Feynman diagrams for a certain scattering process.

Experimentally and theoretically, meson electro- and photoproduction have been well studied in various ways. For instance, in the previous work [4], employing the Rarita-Schwinger formalism for spin-3/2 fermions, it turns out that the contact term interaction, which is responsible for conserving the WT identity, plays a dominant role for the $\Lambda(1520)$ photoproduction. If this is the case, there appears a difference of the production rate between those from the proton and neutron targets related to their isospin structures in each reaction process. Interestingly enough, this theoretical consequence has been confirmed by experiments [5], and supported theoretically [6]. We also note that the formalism used in Refs. [4,7,8] reproduced the presently available data

qualitatively very well [8]. Moreover, the recent beam-energy upgrades of the experimental facilities, such as the CLAS12 at Jefferson Laboratory [10] and the LEPS2 at SPring-8 [11], may shed light on the measurements for new high-energy data for various photo- and electroproduction processes.

In consideration with the success of the theoretical framework employed in Refs. [4,7,8] and the present situation mentioned above, we are motivated to investigate the charged pion ($\pi^\pm$) photoproduction off the proton target with Δ baryon, $\gamma p \to \pi^- \Delta^{++}$ and $\gamma p \to \pi^+ \Delta^0(1232)$, beyond the resonance region $\sqrt{s} \gtrsim 2$ GeV. Although there are other isospin channels in the final $\pi\Delta$ state, we would like to focus on these charge pion productions in the present work because of the abundant experimental data in these specific channels. It is also worth mentioning that these elementary processes are important ingredients to study two-pion photoproduction $\gamma N \to \pi\pi N$. As for the resonance region, the photo- and electroproduction for these elementary-reaction processes were already investigated in Refs. [12,13]. In those works, it turns out that the reaction process contains various contributions, such as those of the Born terms, including the nucleon and baryon resonances, the final- (FSI) and initial-state (ISI) interactions, and the Regge poles. However, as will be shown in the later sections of the present work, only the Born terms and Regge-pole contributions almost saturate the reaction process in the high-energy region beyond the resonance region $\sqrt{s} \gtrsim 2$ GeV. In Ref. [14], the scattering amplitude for $\gamma N \to \pi\Delta$ was also parametrized phenomenologically by a simple one-pion exchange. The Regge poles and absorption corrections were employed for the Δ photoproduction in Ref. [15].

As a theoretical framework, as done in Refs. [7,8], we make use of the effective Lagrangian method and mesonic Regge trajectories. Since we are interested in the energy range beyond the resonance region as mentioned, for simplicity, we will not consider the resonant contributions in the present work. Thus, our strategy to investigate the Δ photoproduction is

[*]sinam@kau.ac.kr
[†]bgyu@kau.ac.kr

quite simple: We take into account the π- and ρ-meson Regge trajectories in the t channel for describing the high-energy experimental data, in addition to the tree-level Born terms, such as the the proton and Δ poles, in the s and u channels, respectively, and contact-term contributions. In treating $\Delta(1232, 3/2^+)$ particles, we make use of the Rarita-Schwinger vector-spinor formalism [16]. In addition to these ingredients, we also take into account an interpolation between the Feynman and Regge propagators by using an ansatz devised for this purpose, which was proved essential to reproduce the low- and high-energy data simultaneously [8]. All the relevant scattering amplitudes are constructed in terms of the tree-level Born approximation without resonant contributions. To consider the spatial distributions of the hadrons involved, we introduce the hadron form factors in a gauge-invariant scheme which preserves the Ward-Takahashi identity with the Regge propagators as done in Refs. [8,17].

From the numerical analyses, we will compute the energy and angular dependences, the polarization-transfer coefficients, and the π^+ decay-angle distribution of the process under various conditions. It turns out that unpolarized physical quantities, such as the energy and angular dependence of the total cross section, are reproduced qualitatively well beyond the resonance region $\sqrt{s} \gtrsim 2$ GeV, as compared to the presently available experimental data. We also discuss the appearance of the strong peak in the forward-scattering region which decreases as the photon energy grows. It turns out that this forward peak is generated by the t-channel pseudoscalar-meson (π) exchange. The angular dependence $d\sigma/dt$ shows that the present framework is not enough to reproduce the experimental data for the region, where $E_\gamma \lesssim 3.5$ GeV and $-t \gtrsim 0.05$ GeV^2. Nevertheless, the present theoretical framework provides very good agreement with the experimental data for the high-energy region beyond $E_\gamma \approx 5$ GeV. In particular, the ansatz for the interpolation of the Feynman-Regge realm plays an important role in reproducing the data appropriately. From the numerical results in the π^+ decay-angle distribution we find in the polarization-transfer coefficients that the ρ-meson exchange, the contact-term contribution, and the π exchange compete with each other in the relatively low-energy region. In contrast, only the ρ-meson exchange and contact-term contribution dominate the process in the high-energy region.

The present work is structured as follows: In Sec. II, we briefly explain the theoretical formalism, such as the effective Lagrangians for the relevant interactions, a gauge-invariant scheme for form factors, and mesonic Regge trajectories to compute the reaction process that we are interested in. Numerical results and related discussions are given in Sec. III. We summarize and close with a conclusion in Sec. IV.

II. FORMALISMS

In this section, we explain the theoretical framework for the present calculations for the $\gamma p \to \pi \Delta$ reaction process. First, we present the relevant Feynman diagrams for the present reaction process at the tree-level Born approximation in Fig. 1. The four momenta of the particles involved are
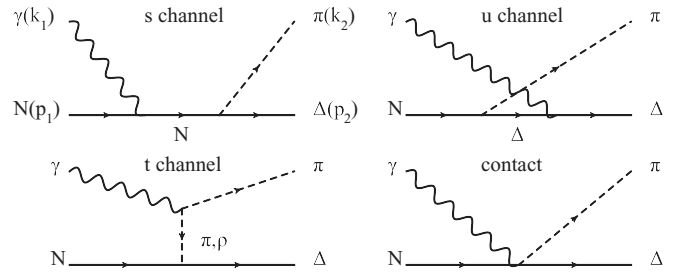

FIG. 1. Relevant Feynman diagrams for the $\gamma N \to \pi \Delta(1232)$ reaction process.

also given there. We will consider the (s, u, t) channel, in which (s, u, t) denotes the Mandelstam variables, and the contact-term contributions. The contact term is necessary for preserving the Ward-Takahashi identity of the scattering amplitude as shown in [4]. The interaction Lagrangians for each vertex are defined as follows:

$$\mathcal{L}_{\gamma PP} = ie_P[(\partial^\mu P^\dagger)P - (\partial^\mu P)P^\dagger]A_\mu + \text{H.c.},$$

$$\mathcal{L}_{\gamma PV} = g_{\gamma PV}\epsilon_{\mu\nu\sigma\rho}(\partial^\mu A^\nu)(\partial^\sigma V^\rho)P + \text{H.c.},$$

$$\mathcal{L}_{\gamma NN} = -\bar{N}\left[e_N A - \frac{e\kappa_N}{4M_N}\sigma^{\mu\nu}F_{\mu\nu}\right]N,$$

$$\mathcal{L}_{\gamma\Delta\Delta} = -\bar{\Delta}^\mu\left[\left(F_1 k g_{\mu\nu} - F_3 k\frac{k_{1\mu}k_{1\nu}}{2M_\Delta^2}\right)\right.$$
$$\left. - \frac{k_1 k}{2M_\Delta}\left(F_2 g_{\mu\nu} - F_4\frac{k_{1\mu}k_{1\nu}}{2M_\Delta^2}\right)\right]\Delta^\nu,$$

$$\mathcal{L}_{PN\Delta} = \frac{g_{PN\Delta}}{M_P}\bar{\Delta}^\mu\partial_\mu P N + \text{H.c.},$$

$$\mathcal{L}_{VN\Delta} = -\frac{ig_{VN\Delta}^{(1)}}{m_V}\bar{\Delta}^\mu\gamma^\nu\gamma_5 V_{\mu\nu}N - \frac{g_{VN\Delta}^{(2)}}{m_V^2}\bar{\Delta}^\mu\gamma_5 V_{\mu\nu}\partial^\nu N$$
$$+ \frac{g_{VN\Delta}^{(3)}}{m_V^2}\bar{\Delta}^\mu\partial^\nu\gamma_5 V_{\mu\nu}N + \text{H.c.},$$

$$\mathcal{L}_{\gamma PN\Delta} = -\frac{ie_N g_{PN\Delta}}{M_P}\bar{\Delta}^\mu A_\mu P N + \text{H.c.}, \quad (1)$$

where e_h stands for the electric charge of the hadron h, whereas e is the unit electric charge. The A, P, V, N, and Δ denote the fields for the photon, pseudoscalar, and vector mesons, nucleon, and $\Delta(3/2^+)$, respectively. The magnetic moment of the proton is $2.79\mu_N$, giving $\kappa_p = 1.79$ for the present case [18]. The antisymmetric tensor is defined by $\sigma = i(\gamma_\mu\gamma_\nu - \gamma_\nu\gamma_\mu)/2$, and $F_{\mu\nu}$ and $V_{\mu\nu}$ are the field-strength tensors for the photon and vector mesons, respectively. The F_{1-4} are the multipole moments of Δ, corresponding to the monopole, dipole, quadrupole, and octupole ones. Since there is no experimental and theoretical information for F_3 and F_4, we will ignore them for brevity in the numerical calculations. As for Δ^{++}, we have $F_1 = e_\Delta$ and F_2, which relates to the magnetic moment $\mu_{\Delta^{++}} = (3.7–8.5)\mu_N$ from the average value of the experimental data [18]. From the theoretical calculations, such as the model-independent way of the chiral quark soliton model (χQSM) [19,20] and the SU(6) quark model [21], it was estimated as $(5.34–5.40)\mu_N$ and $5.58\mu_N$, respectively. Hence, the middle value from

Ref. [18], $5.6\mu_N$, must be a reasonable choice for numerical calculations, resulting in $\kappa_{\Delta^{++}} = 3.6$. The coupling strength of $g_{\pi N \Delta}$ can be computed using the Yukawa vertex, defined by $\mathcal{L}_{PN\Delta}$ in Eq. (1), experimental data of its full decay width $\Gamma_{\Delta \to \pi N} = (116\text{–}120)$ MeV with $\Gamma_\Delta / \Gamma_{\Delta \to \pi N} \approx 100\%$ [22], and the following relation [23]:

$$\Gamma_{\Delta \to \pi N} = \frac{1}{6}\left[\frac{(M_\Delta + M_N)^2 - m_\pi^2}{M_\Delta^2}\right]\frac{g_{\pi N \Delta}^2}{4\pi}\frac{|\boldsymbol{p}_{\pi N}|^3}{m_\pi^2}, \quad (2)$$

where $\boldsymbol{p}_{\pi N}$ indicates the three-momentum of the decaying particle, which can be easily calculated by the Källen function [22]:

$$\boldsymbol{p}_{\pi N} = \frac{\sqrt{[M_\Delta^2 - (M_P + M_N)^2][M_\Delta^2 - (M_P - M_N)^2]}}{2M_\Delta}$$
$$\approx 227 \text{ MeV}. \quad (3)$$

Substituting the experimental information $m_\pi \approx 138$ MeV, $M_N \approx 939$ MeV, and $M_\Delta \approx 1232$ MeV into Eq. (2) and using Eq. (3), one is led to $g_{\pi N\Delta} \approx (2.14\text{–}2.18)$. In numerical calculations, we will make use of $g_{PN\Delta} = 2.16$ as a trial. As for the ρ-meson exchange, the value of $g_{\gamma\rho}$ can be estimated using the interaction Lagrangian in Eq. (1) and the experimental data $\Gamma_{\rho^\pm \to \gamma\pi^\pm} \approx 68.59$ keV; we have it as $0.245/\text{GeV}$ for the charged decay. $g_{VN\Delta}^{(1,2,3)}$ stands for the relevant strong-coupling strengths for each vector-nucleon-Δ vertex. Again, taking into account the limited information on these couplings, we will set them as zero as a trial, except for $g_{VN\Delta}^{(1)} \equiv g_{\rho N\Delta}$. Using a mesonic model, the value of $g_{VN\Delta}^{(1)}$ was determined as $(3.5\text{–}7.8)$ from Ref. [24], and references therein. We will use the average value for it, $g_{\rho N\Delta} = 5.65$ for the numerical calculations.

Using the interaction Lagrangians defined in Eq. (1) for the $\gamma p \to \pi^{(-,+)}\Delta^{(++,0)}$ reaction process, we construct the gauge-invariant amplitudes for the s-, u-, and t-channel contributions:

$$i\mathcal{M}_s = \frac{g_{\pi N\Delta}}{M_\pi}\bar{u}_\mu k_2^\mu \left[\frac{e_N\left[k_1 F_s + (\not{p}_1 + M_N)\hat{F}\right]}{s - M_N^2}\right.$$
$$\left. + \frac{e\kappa_N}{2M_N}\frac{(k_1 + \not{p}_1 + M_N)F_s k_1}{s - M_N^2}\right]\not{\epsilon}u,$$

$$i\mathcal{M}_u = \frac{g_{\pi N\Delta}}{M_\pi}\bar{u}_\mu \not{\epsilon}\left[\frac{e_\Delta[(\not{p}_2 + M_\Delta)\hat{F} - k_1 F_u]}{u - M_\Delta^2}\right.$$
$$\left. + \frac{e\kappa_\Delta}{2M_\Delta}\frac{k_1(\not{p}_2 - k_1 + M_\Delta)F_u}{u - M_\Delta^2}\right]G^{\mu\nu}k_{2\nu}u,$$

$$i\mathcal{M}_c = -\frac{e_\pi g_{\pi N\Delta}}{M_\pi}\hat{F}\bar{u}_\mu \epsilon^\mu u,$$

$$i\mathcal{M}_{t(\pi)} = -\frac{2e_\pi g_{\pi N\Delta}}{M_\pi}\hat{F}\bar{u}_\mu\left(k_1^\mu - k_2^\mu\right)(k_2\epsilon)u\,\mathcal{D}_\pi,$$

$$i\mathcal{M}_{t(\rho)} = \frac{ig_{\gamma\pi\rho}g_{\rho N\Delta}}{M_\rho}F_t\bar{u}_2^\mu\gamma_\nu\left[\left(k_1^\mu - k_2^\mu\right)g^{\nu\sigma} - \left(k_1^\nu - k_2^\nu\right)g^{\mu\sigma}\right]$$
$$\times \left(\epsilon_{\rho\eta\xi\sigma}k_1^\rho\epsilon^\eta k_2^\xi\right)\gamma_5 u_1\,\mathcal{D}_\rho, \quad (4)$$

where k_1, k_2, p_1, and p_2 are the momenta of the photon, pion, proton, and Δ. $\mathcal{D}_{\pi(\rho)} = 1/(t - M_{\pi(\rho)}^2)$ are the t-channel π- and ρ-meson propagators, respectively. $F_{s,u,t}$ stands for the

phenomenological hadronic form factors:

$$F_x = \frac{\Lambda^4}{\Lambda^4 + \left(x - M_x^2\right)^2}, \quad (5)$$

where subscript x stands for the Mandelstam variables [25–27]. The cutoff mass Λ will be determined to reproduce the experimental data in the next section. $G_{\mu\nu}$ denotes the projection operator for the spin-3/2 fermion, assigned as

$$G_{\mu\nu} = g_{\mu\nu} - \frac{1}{3}\gamma_\mu\gamma_\nu - \frac{2}{3M_\Delta^2}q_\mu q_\nu + \frac{q_\mu\gamma_\nu - q_\nu\gamma_\mu}{3M_\Delta},$$
$$q = p_2 - k_1. \quad (6)$$

Although the spin-3/2 propagator was defined above, we will simplify it by setting $G_{\mu\nu} \approx g_{\mu\nu}$, and verify that no significant distinction is observed by this simplification as long as we are interested in the two-body final-state reaction process beyond the resonance region. The $\hat{F}$ indicates a common hadronic form factor to maintain the Ward-Takahashi identity of the scattering amplitude [4,7,8,25–27]:

$$\hat{F} = 1 - (1 - F_s)(1 - F_t)(1 - F_u). \quad (7)$$

We note that this form-factor scheme preserves the gauge invariance, crossing symmetry, and on-shell condition of the form factors. We have verified that the above invariant amplitudes lead to the following charge conservation, satisfying the Ward-Takahashi identity, together with the electric charge in Eq. (4), assigned as $(e_\pi, e_N, e_\Delta) = (-e, +e, +2e)$ and $(+e, +e, 0)$ for the π^- and π^+ photoproductions, respectively.

As mentioned previously, since we are interested in the region beyond that of the resonances, it is necessary to take into account a method to go over the Born approximation, which is believed to be reliable only for the low-energy region. As in Refs. [8,28–31], the Regge-trajectory prescription is one of the most successful and practical methods for this purpose. As for the $\gamma p \to K^+\Lambda(1520)$ photoproduction [8], whose threshold energy is about $E_\gamma \approx 1.67$ GeV, the Regge contribution becomes significant beyond $E_\gamma \approx 4$ GeV. Furthermore, the Regge contribution turns out to be responsible for reproducing the angular dependence of the scattering process correctly, especially for the momentum-transfer t dependence, i.e., $d\sigma/dt$ in the high-energy region.

In the present work, we will consider the Regge trajectories for the pion and ρ meson in the t channel. However, for simplicity, we will not consider the axial-vector and tensor mesons, such as $a_1(1260, 1^+)$, $b_1(1235, 1^+)$, $a_2(1320, 1^+)$, and so on. As discussed in Refs. [8,9], the prescription for the reggeization can be applied to the present framework by replacing the t-channel Feynman propagators in the invariant amplitudes in Eq. (4) with the following one:

$$\mathcal{P}_X = \frac{\pi\alpha_X'}{\Gamma[\alpha_X(t) - J_X + 1]\sin[\pi\alpha_X(t)]}\left(\frac{s}{s_0}\right)^{\alpha_X(t) - J_X},$$
$$\alpha_X(t) = J_X + \alpha_X'(t - m_X^2)\text{ GeV}^{-2}, \quad (8)$$

where α_X denotes the Regge trajectory for meson X as a function of t with slope α_X'. J_X and m_X stand for the spin and mass of the meson, respectively. Here is a caveat; in deriving Eq. (8), all the even and odd spin trajectories are assumed

TABLE I. Relevant inputs for the Regge trajectory of the meson X.

	J^P	m_X	J_X	α'_X
π	0^-	140 MeV	0	0.7
ρ	1^-	770 MeV	1	0.8

to be degenerate, although in reality these trajectories are not degenerated [29–31]. Moreover, for convenience, we have set the phase factor for the propagators to be positive unity as done in Ref. [17]. The cutoff parameter s_0 is chosen to be 1 GeV conventionally [29–31]. Since the gamma function in Eq. (8) plays the role of the form factor in the Feynman propagator to suppress the divergence of the Regge propagator at the singularities $\sin[\pi\alpha_X(t)] = 0$, we will not consider the form factors given in Eq. (4), setting all of them to unity in the Regge-pole calculation. Hereafter, we use a notation $i\mathcal{M}^{\text{Regge}}$ for the amplitude thus constructed with the Regge propagators in Eq. (8). We list the relevant inputs for the Regge trajectories in Table I.

Let us now discuss gauge invariance of the present invariant amplitude where the π and ρ exchanges in Eq. (4) are reggeized with the Regge propagators in Eq. (8). Following the procedure in Refs. [29–31] for the t-channel reggeization, we write the reggeized amplitude for the π exchange as

$$i\mathcal{M} = i\mathcal{M}^{\text{Regge}}_{t(\pi,\rho)} + (i\mathcal{M}_s + i\mathcal{M}_u + i\mathcal{M}_c). \quad (9)$$

It is, then, easy to show that the amplitude in Eq. (9) does not satisfy the current conservation as follows:

$$k_1(i\mathcal{M}) = k_1\left(i\mathcal{M}^{\text{Regge}}_{t(\pi)} + i\mathcal{M}^E_s + i\mathcal{M}^E_u + i\mathcal{M}_c\right) \neq 0. \quad (10)$$

Hence, the sum of the π exchange in t-channel and electric s and u channels must be zero to satisfy the gauge invariance, whereas the ρ exchange and magnetic contributions are automatically zero, due to their antisymmetric nature. To satisfy the gauge invariance, we follow the prescription in Refs. [29–31] as

$$i\mathcal{M}^{\text{Regge}}_{t(\pi)} + i\mathcal{M}^E_s + i\mathcal{M}^E_u + i\mathcal{M}_c$$
$$\rightarrow i\mathcal{M}^{\text{Regge}}_{t(\pi)} + \left(i\mathcal{M}^E_s + i\mathcal{M}^E_u + i\mathcal{M}_c\right)\left(t - m_\pi^2\right)\mathcal{P}_\pi$$
$$\equiv i\bar{\mathcal{M}}^{\text{Regge}}, \quad (11)$$

where we set $F_{s,u}$ and $\hat{F}$ to be unity for the $i\bar{\mathcal{M}}^{\text{Regge}}$. Thus, the reggeized amplitude can be written as follows:

$$i\mathcal{M} = i\bar{\mathcal{M}}^{\text{Regge}} + i\mathcal{M}^M_s + i\mathcal{M}^M_u + i\mathcal{M}^{\text{Regge}}_{t(\rho)}, \quad (12)$$

where superscript M denotes the magnetic contributions of the s and u channels.

Considering that the Regge propagators work properly for $(s, |t|) \rightarrow (\infty, 0)$ and assuming that the Regge contributions can survive even in the low-energy region $(s, |t|) \rightarrow (s_{\text{threshold}}, \text{finite})$, it is natural to expect a smooth interpolation between two regions. Hence, it is physically natural to consider that the meson propagators are supposed to smoothly shift from the Regge one for $s \gtrsim s_{\text{Regge}}$ to a usual Feynman one for $s \lesssim s_{\text{Regge}}$. Here, s_{Regge} indicates a certain value of s from which the Regge contributions become effective. Moreover, it is also likely that the interpolation reveals unknown production

mechanisms parametrically in the intermediate energy region. As discussed in Ref. [8] in detail, there is no unique scheme to interpolate these two regions. Thus, as a trial, we introduce a Feynman-Regge interpolating ansatz by redefining the form factors in the relevant invariant amplitudes in Eq. (4) as follows:

$$\hat{F} \rightarrow \bar{F}_c \equiv \left[(t - M_X^2)\mathcal{P}_X\right]\mathcal{R} + \hat{F}(1 - \mathcal{R}), \quad (13)$$

where

$$\mathcal{R} = \frac{1}{2}\left[\tanh\left(\frac{s - s_{\text{Regge}}}{s'}\right) + 1\right]. \quad (14)$$

Here, s' denotes a free parameter to make the argument of tanh in Eq. (14) dimensionless. It is easy to understand that $\mathcal{R}$ goes to unity as $s \rightarrow \infty$ and approaches zero as $s \rightarrow 0$. This asymptotic behavior of $\mathcal{R}$ ensures that $\bar{F}_c$ in Eq. (13) interpolates the two energy regions smoothly. As already shown in Ref. [8], this interpolating description works qualitatively very well in reproducing the low- and high-energy region data simultaneously. We will determine the parameters s_{Regge} and s' with experimental data in the next section.

As discussed above, we have three different models in the following sections, assigned as

(1) *Born*: The scattering amplitude is defined with the conventional Born propagators with the phenomenological form factors as in Eqs. (4), (5), and (7).

(2) *Regge*: The scattering amplitude is modified by the Regge contributions without form factors as in Eq. (12).

(3) *Interpolation*: The Regge approach is modified by the interpolation formula in Eqs. (13) and (14).

III. NUMERICAL RESULTS AND DISCUSSIONS

In this section, we present the numerical results for the various physical observables such as the energy and angular dependences of the cross sections for the two charged pion photoproduction processes. We also show the numerical results for the polarization-transfer coefficient ($C_{x,z}$) [7,32,33] and the π^+-decay angle distribution [8,34] for the $\gamma p \rightarrow \pi^- \Delta^{++}$ process, in addition to the photon-beam asymmetry with the linearly polarized beam. The results are compared with experimental data to provide theoretical estimations useful for future experiments.

First, we investigate the unpolarized total cross section as a function of the photon energy E_γ in the three different models, using the cutoff mass $\Lambda = 450$ MeV. We present the results for the π^- photoproduction in panel (a) of Fig. 2 in which the solid, dotted, and dot-dashed lines correspond to the Born, Regge, and interpolation models, respectively. The experimental data are taken from Refs. [35–37]. The simple Born method provides qualitatively good agreement with the data, whereas the Regge one corresponding to $\mathcal{R} = 1$ shows overshoot in the lower-energy region. This observation indicates that the simple replacement of the t-channel Feynman propagators with the Regge ones in the present case does not work very well. In the application of the interpolation ansatz with the relevant parameters determined as $s_{\text{Regge}} = (3.5 \text{ GeV})^2$ and $s' = (2.5 \text{ GeV})^2$, we obtain a
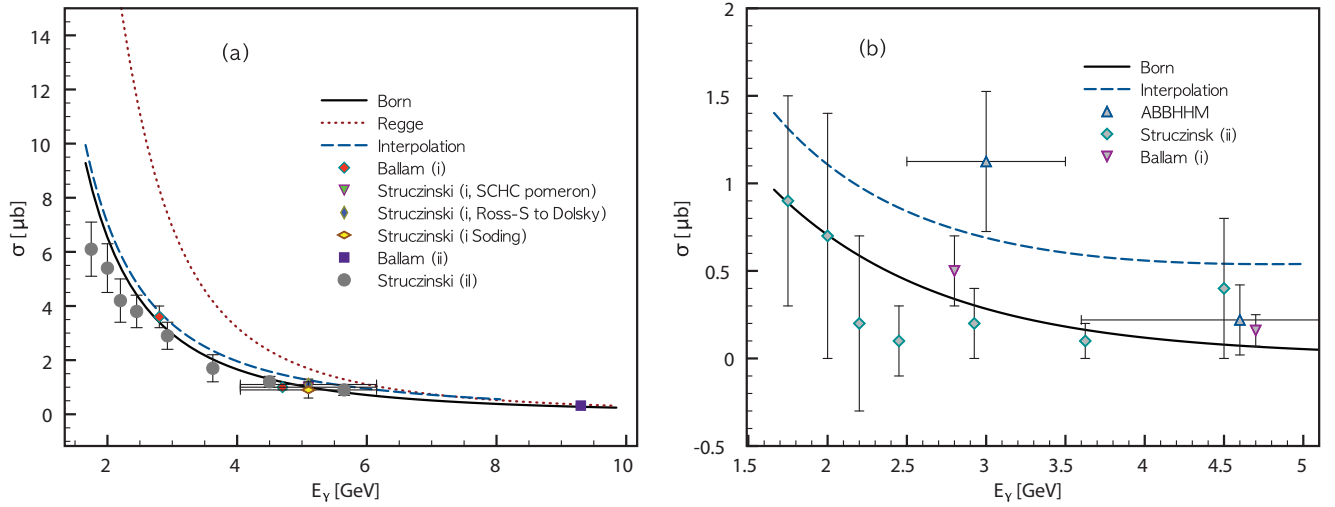
FIG. 2. (Color online) Total cross sections for the $\gamma p \to \pi^- \Delta^{++}$ (a) and $\gamma p \to \pi^+ \Delta^0$ (b) reaction processes as a function of E_γ. Experimental data are taken from Refs. [35] [Ballam (i)], [36] [Struczinski (i)], [37] [Ballam (ii)], [42] [Struczinski (ii)], and [43] (ABBHHM). We show the curves from the numerical results for the Born terms (solid), that plus the Regge (dotted), those with the interpolation (dashed), separately. For more details, see the text.

reasonable result as shown in panel (a) of Fig. 2. These values indicate that the Regge contribution starts to prevail over the present reaction process beyond $\sqrt{s} \approx 3.5$ GeV. Note that the cutoff mass $\Lambda = 450$ MeV used for the present calculation is about 25% smaller than that for the $\Lambda(1520)$ photoproduction [4,7,8]. As for the π^+ photoproduction, it turns out that one needs much smaller cutoff mass to reproduce the experimental data qualitatively, i.e., $\Lambda \approx 200$ MeV as shown in panel (b) of Fig. 2 for the Born and interpolation models. Note that this cutoff value is much smaller than that for the π^- photoproduction, indicating that there can be considerable contributions beyond those from the ground-state hadrons. The numerical results for the Born and interpolation models show similar energy dependence, whereas their strengths are

rather different, although the experimental data contain sizable uncertainties in this channel. Note that the Regge-model result strongly overshoots the data, which are not depicted here.

Panel (a) of Fig. 3 shows the differential cross section for the π^- photoproduction as a function of E_γ for the three different angles, $\theta = (0, 30°, 60°)$ with the same notations for the lines as those in Fig. 2. At the very forward angle $\theta = 0$, the strength of the cross section decreases monotonically for the three cases without showing significant differences. On the contrary, as the angle increases, the difference between them becomes obvious, according to the considerable contributions of the Regge ones. By applying the interpolation ansatz, the difference between the models with and without the interpolation turns out to be moderate for $\theta \gtrsim 30°$, and becomes negligible
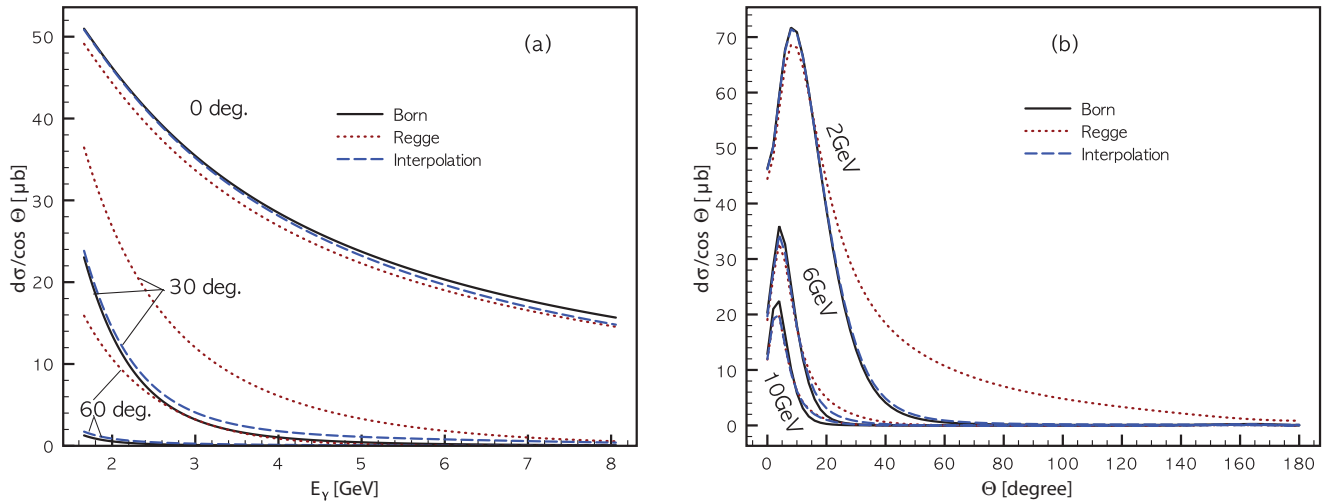

FIG. 3. (Color online) Differential cross section for $\gamma p \to \pi^- \Delta^{++}$ as a function of E_γ for different angles $\theta = (0, 30°, 60°)$ for the Born terms (solid), that plus the Regge (dotted), and those with the interpolation (dashed), separately in (a). In (b) we plot the differential cross section as a function of θ for different energies, $E_\gamma = (2, 6, 10)$ GeV, represented in the same manner as (a).

at $\theta = 60°$. In panel (b) of Fig. 3, we draw the differential cross section as a function of θ for different energies, $E_\gamma = (2, 6, 10)$ GeV, represented in the same manner as panel (a). From this we can conclude that there is strong t-channel contribution, which makes a peak in the forward-scattering region. This tendency is rather different from that of the $\Lambda(1520)$ photoproduction, in which case the contact-term contribution dominates the reaction process [4,7,8]. As the energy increases, the overall strength of the differential cross sections becomes smaller and the peak position moves to the vicinity around $\theta = 0$. We will discuss the shift of the peak position in detail below. We note that the Born and interpolation models provide almost negligible contributions in the backward-scattering region, $\theta \gtrsim 60°$, which can be understood easily from panel (a) in Fig. 3: the smaller strengths for the larger angles.

Now we are in a position to discuss the momentum-transfer t dependence of the present reaction process, represented by $d\sigma/dt$ as a function of $-t$ for the π^- photoproduction, as in Fig. 4. The three cases for the Born (a), Regge (b), and interpolated (c) models are presented separately for the four different energy ranges; $E_\gamma = 2.4$–2.8 GeV, $E_\gamma = 2.8 - 3.6$ GeV, $E_\gamma = 3.6$–4.4 GeV, and $E_\gamma = 4.4$–4.8 GeV, in which the shaded band stands for each energy interval. The experimental data are taken from Ref. [38]. As for the Born model (a) in Fig. 4, the experimental data are qualitatively well reproduced in the region $-t = (0.05$–$0.2)$ GeV^2. Outside the region, only the high-energy data around $E_\gamma \approx 4.6$ GeV are in relatively good agreement with the theoretical prediction. In other words, these observations tell us that there can be missing contributions for the lower-energy region in the present framework, especially for the small $|t|$ region. Such discrepancies indicate the need for further contributions from the N and Δ resonances around $\sqrt{s} = (2$–$3)$ GeV and possibly from other kinds of t-channel meson exchanges which we are not considering here. As we take into account the Regge contributions as shown in Fig. 4(b), there appears strong enhancement for the region beyond $-t \gtrsim 0.2$ GeV^2, which overshoots the data. Again, this unexpected overestimation is tamed by including the interpolating ansatz as seen in Fig. 4(c), which leads to relatively good agreement with the experimental data. In Fig. 4(d) we draw each contribution separately for the $d\sigma/dt$ at $E_\gamma = 2.4$ GeV, using the Born model, in order to see which contribution is essential to produce the curve. As shown, the π-exchange and contact-term contributions dominate the forward-scattering region, whereas the others are considerably small. Moreover, one can easily see that the contact-term contribution makes the peak shift to the smaller t region ($-t \approx 0.01$ GeV^2). By comparing this observation with Fig. 3(b) and seeing the shift of the peak, one can easily find that the contact-term contribution prevails over the π exchange as E_γ increases, although the contribution of the π exchange is still manifesting. In Fig. 4(e), we also show the numerical results, using the interpolation model, for the π^+ photoproduction. Again, we observe similar tendency with that for the π^- case.

In Fig. 5, we present the numerical results of the momentum-transfer t dependence for the higher photon-energy regions, $E_\gamma = 5$ (a), 8 (b), 11 (c), and 16 (d) GeV. The experimental data are taken from Refs. [39–41]. Similarly,

we draw the three models, Born (solid), Regge (dotted), and interpolation (dashed), separately. It can be clearly seen that the one with the interpolation yields considerably excellent results in comparison with the experiment. We also find that the results from the Born approximation are only reliable below $-t \approx 0.1$ GeV^2 for all the photon energies. Beyond this value, we observe that the Regge contribution plays a critical role, as shown in Fig. 5. At the same time, the interpolation ansatz works very well for these relatively high-energy ranges. For instance, we see that the value of $\mathcal{R}$ becomes about 0.4, which indicates that the contributions from the Regge and Feynman propagators are almost in the same portion for $E_\gamma = 5$ GeV. As expected, with a much higher energy such as $E_\gamma = 16$ GeV, the $\mathcal{R}$ becomes almost unity, i.e., the Regge propagator prevails almost completely over the Feynman one. Hereafter, we will show the numerical results only from the interpolation case, since we have seen that the ansatz for the interpolation has reproduced the experimental data qualitatively very well so far. As for the π^+ photoproduction, we again find a qualitative agreement with the data as shown in Fig. 5(e), although sizable deviation is observed in comparison to that for the π^- one.

Now we discuss the polarized quantities for the Δ^{++} photoproduction, such as the polarization-transfer coefficients $C_{x,z}$. Among the polarization observables in a meson photoproduction, C_x and C_z are identified as the spin asymmetry along the direction of the polarization of the recoil baryon with the circularly polarized photon beam. First, we define the polarization-transfer coefficients in the (x', y', z') coordinate, being similar to those for the spin-1/2 hyperon-photoproduction as in Refs. [32,33]:

$$C_{x',|S_{x'}|} = \frac{\frac{d\sigma}{d\Omega}_{r,0,+S_{x'}} - \frac{d\sigma}{d\Omega}_{r,0,-S_{x'}}}{\frac{d\sigma}{d\Omega}_{r,0,+S_{x'}} + \frac{d\sigma}{d\Omega}_{r,0,-S_{x'}}},$$
$$C_{z',|S_{z'}|} = \frac{\frac{d\sigma}{d\Omega}_{r,0,+S_{z'}} - \frac{d\sigma}{d\Omega}_{r,0,-S_{z'}}}{\frac{d\sigma}{d\Omega}_{r,0,+S_{z'}} + \frac{d\sigma}{d\Omega}_{r,0,-S_{z'}}},$$
(15)

where subscripts r, 0, and $\pm S_{x',z'}$ stand for the right-handed photon polarization, unpolarized target nucleon, and polarization of the recoil baryon along the x' or z' axis, respectively. Since the photon helicity is fixed to be $+1$ here, $C_{x'}$ and $C_{z'}$ measure the polarization transfer to the recoil baryon. Moreover, $C_{x'}$ and $C_{z'}$ behave as the components of a three-vector so that it can be rotated to the (x, y, z) coordinate as

$$\begin{pmatrix} C_x \\ C_z \end{pmatrix} = \begin{pmatrix} \cos\theta_K & \sin\theta_K \\ -\sin\theta_K & \cos\theta_K \end{pmatrix} \begin{pmatrix} C_{x'} \\ C_{z'} \end{pmatrix},$$
(16)

where the (x, y, z) coordinate stands for when the incident photon momentum is aligned with the z axis. These polarization quantities were already investigated for the spin-1/2 [33] and spin-3/2 [7,8] baryons. The numerical results for $C_{x,z}$ are presented in Fig. 6, employing the interpolation mode only, for different E_γ values, (2–12) GeV corresponding to panels (a)–(f). All the results show $C_z = 1$ and $C_x = 0$ in the collinear limit, i.e., at $\cos\theta = \pm 1$, due to the helicity conservation. Generally, we observe very complicated structures for the vicinity
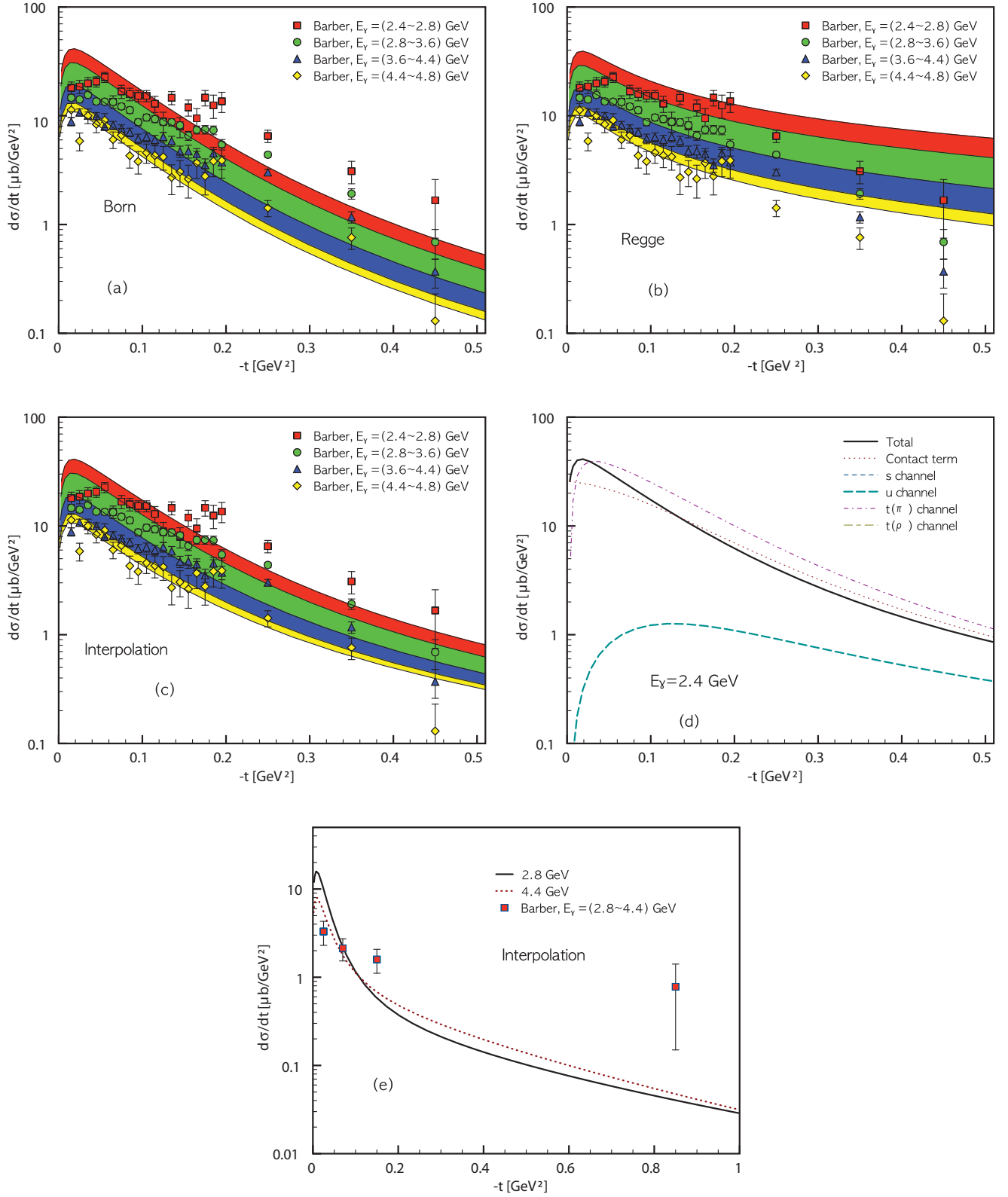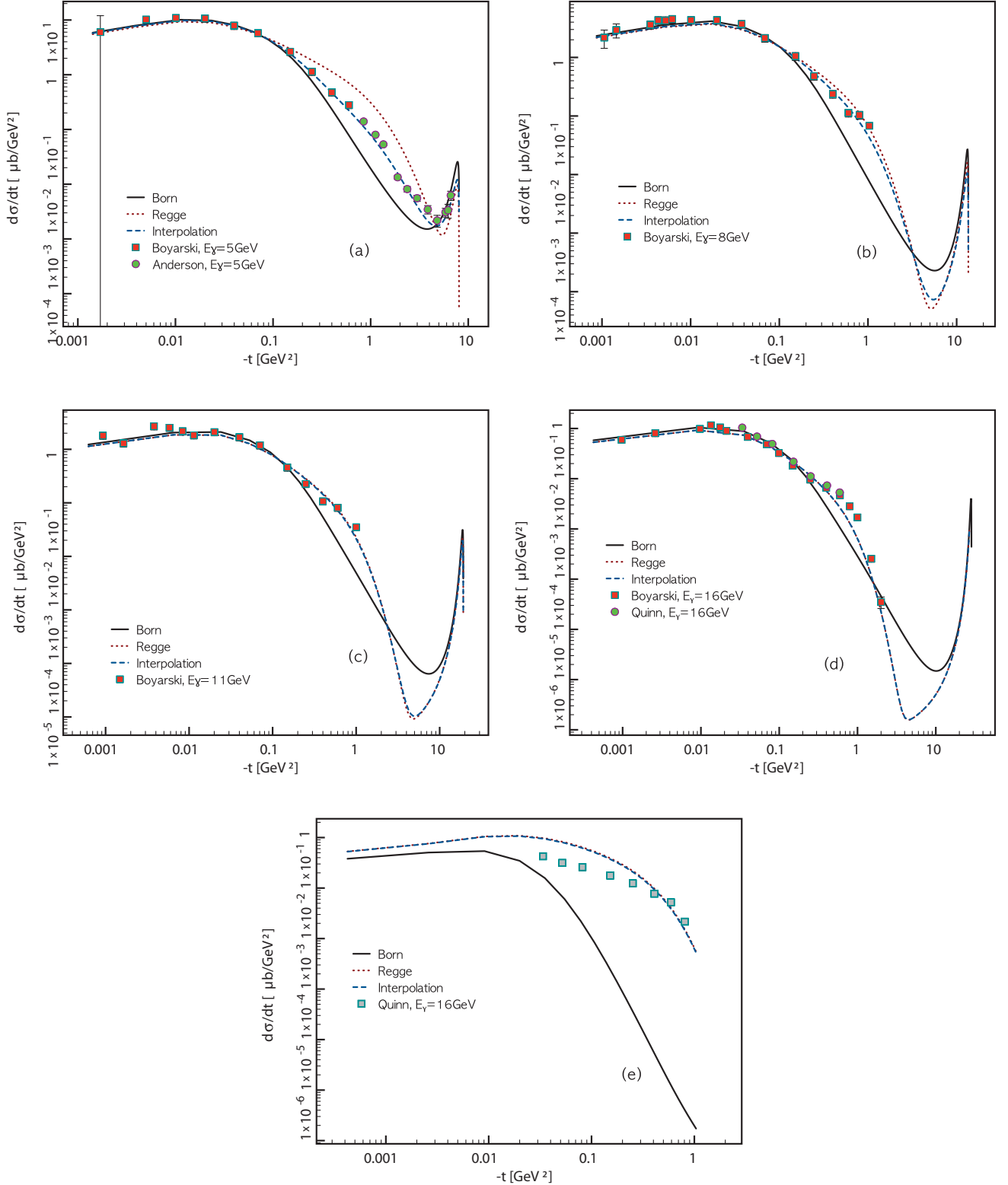
FIG. 4. (Color online) Angular dependence $d\sigma/dt$ [μb/GeV^2] for $\gamma p \to \pi^- \Delta^{++}$ as a function of $-t$ (GeV^2) for the low-energy region $E_\gamma = (2.4$–$4.8)$ GeV for the Born terms (a), that plus the Regge (b), and those with the interpolation (c), separately. Experimental data are taken from Ref. [38] (Barber). Each contribution is also drawn for $E_\gamma = 2.4$ GeV (d). In (e) we draw the numerical result for the $\gamma p \to \pi^+ \Delta^0$, using only the interpolation model.

FIG. 5. (Color online) (Color onnline) Angular dependence $d\sigma/dt$ (μb/GeV^2) for $\gamma p \to \pi^- \Delta^{++}$ as a function of $-t$ (GeV^2) for the high-energy region $E_\gamma = (5, 8, 11, 16)$ GeV in (a), (b), (c), and (d), respectively. Experimental data are taken from Refs. [39] (Boyarski), [40] (Anderson), and [41] (Quinn). In (e) we draw the numerical result for the $\gamma p \to \pi^+ \Delta^0$.

cos $\theta \gtrsim 0.5$, because of complicated interferences between the π-exchange and contact-term contributions. For $E_\gamma \gtrsim 8$ GeV, the shapes of the curves remain relatively unchanged. This tendency, negligible changes for the higher photon energies,
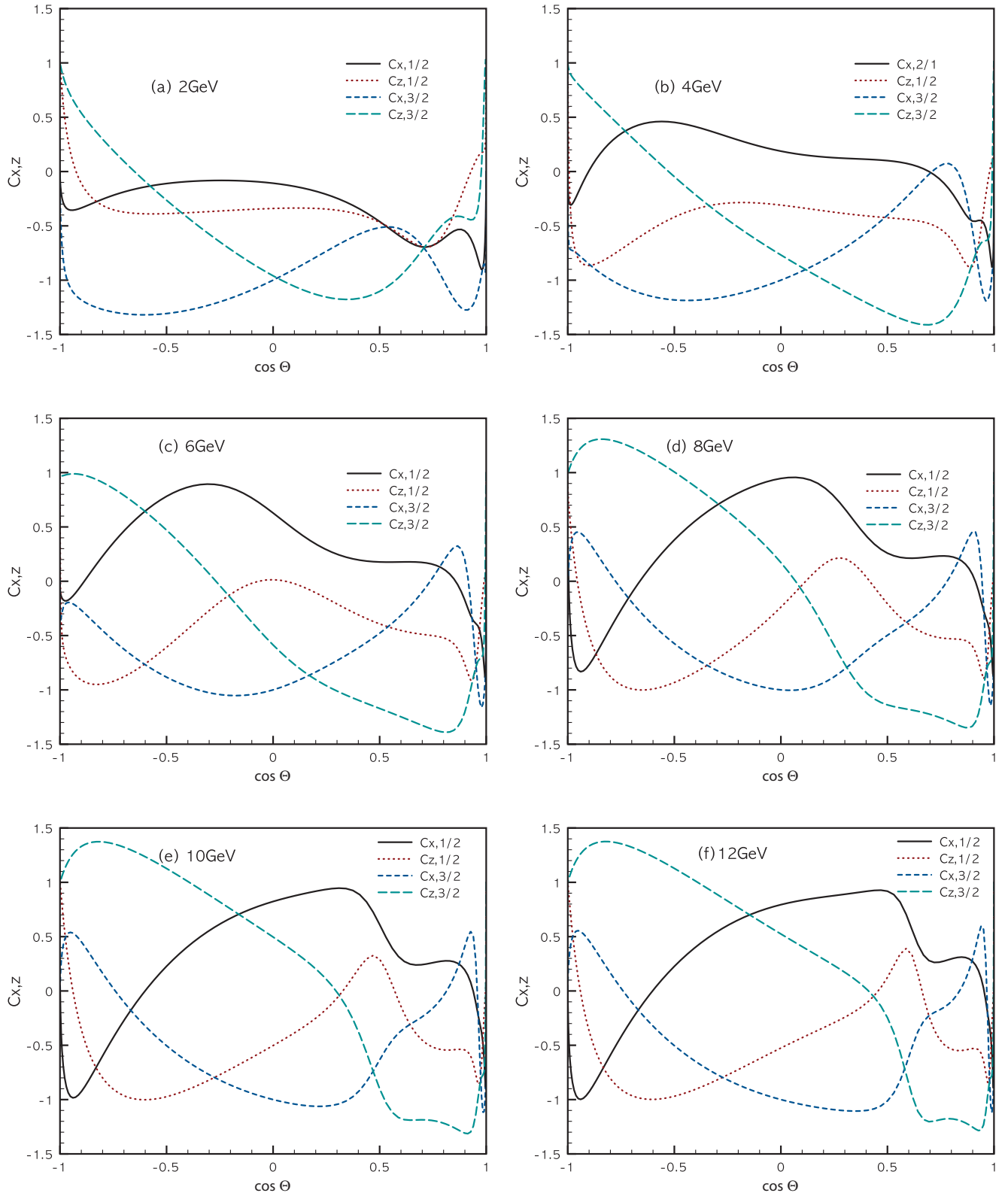
FIG. 6. (Color online) Polarization-transfer coefficients $C_{x,z}$ for the spin-1/2 and -3/2 components for $\gamma p \rightarrow \pi^- \Delta^{++}$ as functions of $\cos \theta$ for different photon energies, $E_\gamma = (2\text{--}12)$ GeV, corresponding to panels (a)–(f), computed from the interpolation model.

was already observed for the $\Lambda(1520)$ photoproduction [7,8]. We expect that $C_{x,z}$ for the Δ photoproduction at high

energy can be measured by CLAS Collaboration at Jefferson Laboratory, considering their upgraded photon-beam energy
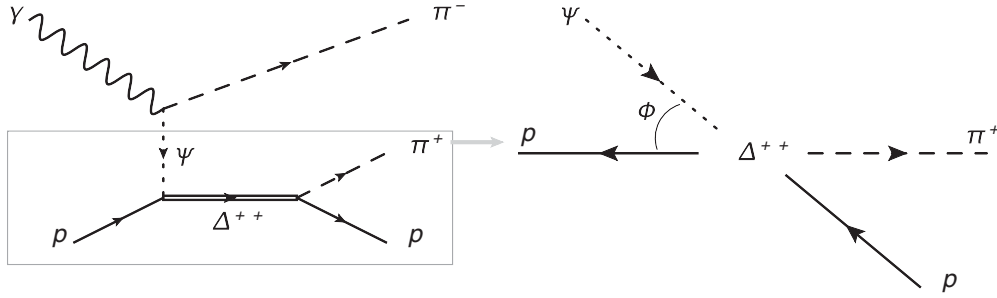
FIG. 7. (Left) Feynman diagram for $\gamma p \to \pi^+ \pi^- p$. In the box, the subsequent process, $\psi p \to \Delta^{++} \to \pi^+ p$, is depicted, where ψ indicates a meson exchanged. The diagram in the box can be interpreted using the Gottfried-Jackson frame as shown on the right. The angle ϕ is defined by that between the initial and final particles.

and high performance of the circular photon polarization, as already done for the ground-state Λ hyperon, i.e., $\Lambda(1116)$ [32].

In regard to $C_{x,z}$, we want to discuss the π^+ decay-angle distribution function for the π^- photoproduction process. The decay-angle distribution has already been discussed experimentally for the $\Lambda(1520)$ photoproduction [34,44]. Theoretically, it was also explored in the previous work [7,8]. The decay-angle distribution is the angle distribution of π^+ that decays via $\Delta^{++} \to \pi^+ p$ in the t-channel helicity frame, i.e., the Gottfried-Jackson frame [45]. Schematic figures for this frame and kinematics are shown in Fig. 7, wherein the decay angle ϕ is defined. From this distribution function one can see which meson exchange is dominating the production process. According to the spin statistics, the distribution function becomes proportional to $\sin^2 \phi$ for Δ^{++} in $S_z = \pm 3/2$, whereas $\frac{1}{3} + \cos^2 \phi$ for Δ^{++} in $S_z = \pm 1/2$. As in Refs. [44,46], considering all the possible contributions, we can parametrize the distribution function as follows:

$$\mathcal{F}_{\pi^+} = A \sin^2 \phi + B \left(\tfrac{1}{3} + \cos^2 \phi \right), \quad (17)$$

where we have used a notation $\mathcal{F}_{\pi^+}$ indicating the distribution function for convenience. The coefficients A and B stand for the strength of each spin state of Δ^{++} with the normalization condition $A + B = 1$. In other words, if $A > B$, one can think

that the spin-1 particle exchange or an equivalent contribution in the t channel dominates the scattering process, and vice versa for the spin-0 particle exchange. We note that there can be other N^* and/or Δ^* contributions in addition to Δ^{++}, so that one can add an additional term to Eq. (17) representing the interference effects. However, we will ignore this for simplicity, as in Refs. [7,8].

Now we provide theoretical estimations on $\mathcal{F}_{\pi^+}$. Note that we again only show the numerical results for the interpolation model hereafter. Since the outgoing pion (π^-) carry no spin, all the photon helicity will be transferred to Δ^{++} through the exchanging particle in the t channel, Hence, it is natural to think that the polarization-transfer coefficients in the z direction should relate to the strength coefficients A and B. Therefore, we can write A and B in terms of $C_{z,1/2}$ and $C_{z,3/2}$ as follows:

$$A = \frac{C_{z,3/2}}{C_{z,1/2} + C_{z,3/2}}, \qquad B = \frac{C_{z,1/2}}{C_{z,1/2} + C_{z,3/2}}, \quad (18)$$

which satisfy the normalization condition. In other words, A denotes the strength that Δ^{++} is in its $S_z = \pm 3/2$ state, and B for $S_z = \pm 1/2$. In Fig. 8, we depict it as a function of ϕ for different $\theta = (10\text{–}50)^\circ$ and $E_\gamma = 3$ and 9 GeV in panels (a) and (b), respectively. As for the lower energy ($E_\gamma = 3$ GeV), the numerical results tell us that the scattering
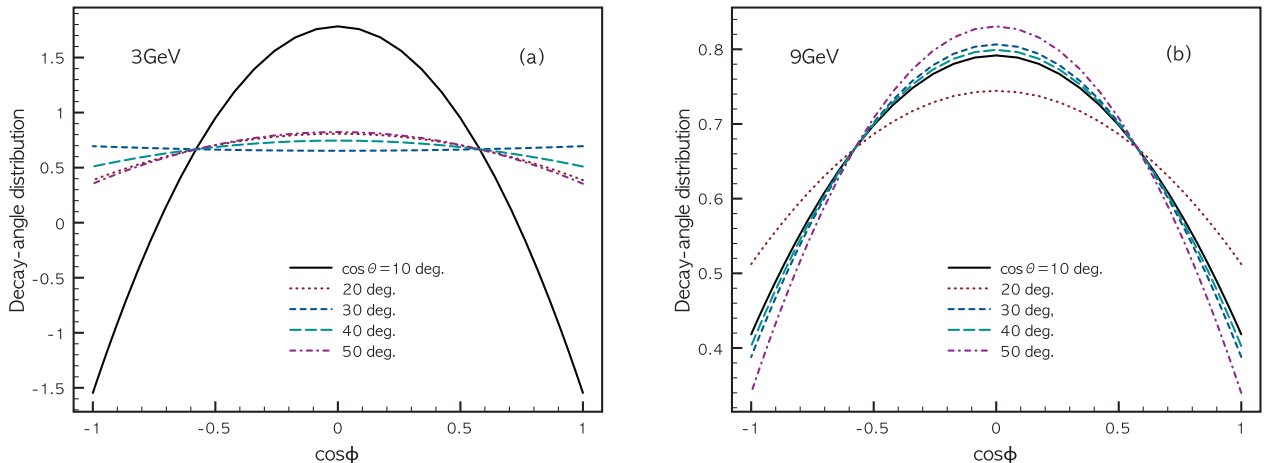

FIG. 8. (Color online) Decay-angle distribution for $\gamma p \to \pi^- \Delta^{++}$ for the π^+ as a function of $\cos \phi$, which is the angle between the p and π^+ decaying from the Δ^{++} in the Gottfried-Jackson frame, for two different photon energies $E_\gamma = 3$ and 9 GeV in (a) and (b), respectively.
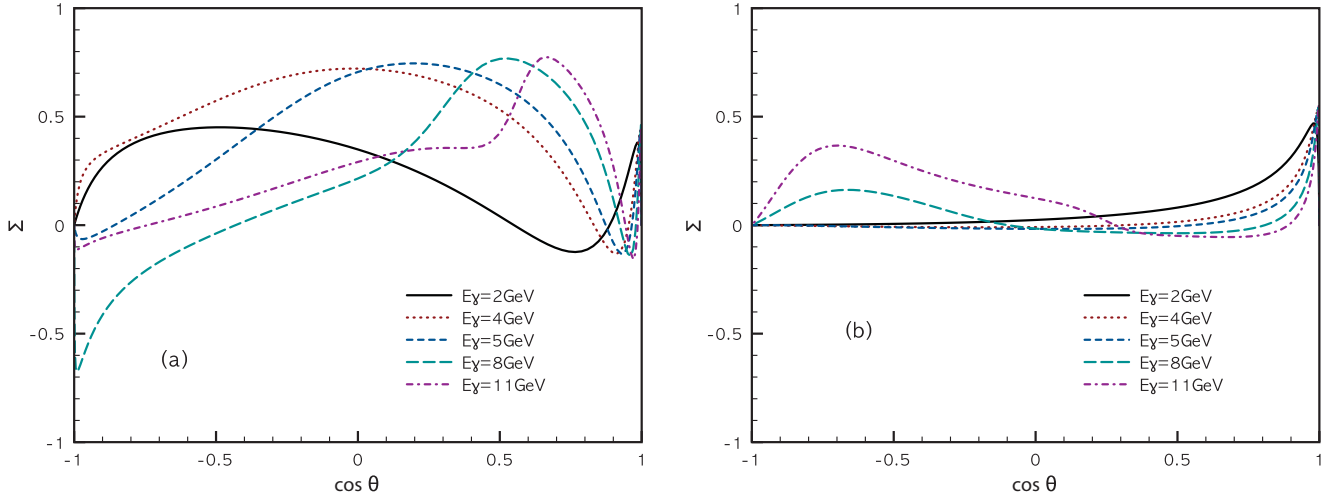
FIG. 9. (Color online) Photon-beam asymmetry Σ defined in Eq. (19) as a function of $\cos\theta$ for $\gamma p \to \pi^- \Delta^{++}$ (a) and $\gamma p \to \pi^+ \Delta^0$ (b) for various photon energies, $E_\gamma = (2\text{--}11)$ GeV, using the same model parameters with the above calculations.

process is mainly dominated by the spin-1 exchange or equivalent contribution for the very forward-scattering angles. Moreover, this observation indicates that the contact-term contribution dominates the process, since it can be interpreted equivalently as a spin-1 exchange, and the contact-term one is more effective than that of the ρ exchange, as discussed above. However, for the angle around $\theta = 30°$, the spin-0 exchange, i.e., π-meson exchange, contributes significantly as denoted by the short-dashed line in Fig. 8(a). Beyond that angle, again, the contact-term contribution prevails over that from the spin-0 one. As for the higher-energy region, the situation becomes quite different from the lower-energy case. In Fig. 8 we show the decay-angle distribution for $E_\gamma = 9$ GeV. We see that for all the π^- angles, the contact-term contribution dominates the process, in addition to the tiny ρ-meson exchange one, as understood from Fig. 4(d).

Finally, in the present work we explore a single-polarization observable, i.e., the photon-beam asymmetry Σ, defined by the following [4,47,48]:

$$\Sigma = \frac{d\sigma_\parallel - d\sigma_\perp}{d\sigma_\parallel + d\sigma_\perp}, \qquad (19)$$

where $d\sigma_\parallel$ and $d\sigma_\perp$ represent the differential cross sections with the polarized photon beam parallel and perpendicular to the reaction plane, respectively. From this definition, pure π-exchange amplitude gives $\Sigma = 1$. Note that this physical quantity can be measured by the experiments, such as LEPS and CLAS Collaborations, in comparison to the double polarizations as discussed above. In Fig. 9, we present the numerical results for Σ as a function of $\cos\theta$ for $\gamma p \to \pi^- \Delta^{++}$ in panel (a) and $\gamma p \to \pi^+ \Delta^0$ in panel (b) for various photon energies, $E_\gamma = (2\text{--}11)$ GeV, using the same model parameters as the above calculations. As for the π^- photoproduction in Fig. 9(a), we observe that a bump moves toward the region around $\cos\theta = 1$, i.e., the forward-scattering region, as the energy increases. We verified that this tendency originated dominantly from the nontrivial interference between the contact-term and t-channel contributions. On the contrary, we

have no u-channel contribution for the π^+ photoproduction, as long as the resonances are not taken into account in the present work. Moreover, since there is a sign difference in the electric coupling for the t-channel contributions between the processes, the Σ curves for the π^+ photoproduction, as shown in Fig. 9(b), represent quite different shapes in comparison to those for the π^- photoproduction. It turns out that, even for the π^+ photoproduction, the contact-term and t-channel contributions play a crucial role in shaping the curves.

IV. SUMMARY AND CONCLUSION

In the present work, we have investigated the photoproduction of the charged pion with the $\Delta(1232, 3/2^+)$ baryon off the proton target at tree level, using the effective Lagrangian approach, beyond the resonance region. We took into account the nucleon- and Δ-pole diagrams corresponding to s- and u-channel contributions, respectively. The π and ρ exchanges are considered in the t channel. For the gauge invariance of the scattering amplitude, the contact-term contribution was further included together with the gauge-invariant scheme for the form factors. The Regge trajectories for the π and ρ mesons are introduced to describe the high-energy experimental data correctly. We introduced an ansatz designated to interpolate the Feynman and Regge propagators. These three different cases were assigned as the Born, Regge, and interpolation models. It turned out that the present numerical results are in good agreement with the experimental data and could provide useful theoretical guides and estimations for future experiments. We list the important observations in the present work as follows:

(1) Unpolarized physical quantities such as the energy and angular dependences of the cross sections are reproduced qualitatively well beyond the resonance region $\sqrt{s} \gtrsim 2$ GeV for the interpolation model, in comparison to the presently available experimental data.

(2) We observe a strong peak in the forward-scattering region. It is suppressed with respect to E_γ. It also turns out that this forward peak is generated by the t-channel

pseudoscalar-meson (π) exchange on top of the subleading contact-term contribution, although the latter gets stronger as E_γ increases. In general, the peak shifts to the very forward region as E_γ increases.

(3) The angular dependence $d\sigma/dt$ shows that the present framework is not enough to reproduce the experimental data for regions $E_\gamma \lesssim 3.5\,\mathrm{GeV}$ and $-t \gtrsim 0.05\,\mathrm{GeV}^2$. The observed discrepancy may indicate the necessity of the further unknown contributions from the higher-spin meson exchanges in the t channel as well as the higher-mass baryon resonances, though not taken into account in the present work.

(4) On the contrary, the present theoretical framework provides very good agreement with the experimental data for the high-energy region beyond $E_\gamma \approx 5\,\mathrm{GeV}$. In particular, the ansatz for the Feynman-Regge interpolation plays an important role in reproducing the data appropriately.

(5) We also present the numerical results for one of the various double polarization observables, i.e., the polarization-transfer coefficients $C_{x,z}$. With the collinear-limit conditions for the region $E_\gamma \gtrsim 8\,\mathrm{GeV}$, $C_{x,z}$ remains almost unchanged, whereas nontrivial structures are shown at the forward-scattering regions due to interference between the contact term and π exchange.

(6) From the numerical results in the π^+ decay-angle distribution function, we find that in the low-energy region the spin-1 exchange (small ρ-meson exchange plus the large contact-term contribution) and that of spin-0 (π exchange) compete with each other, depending on the θ angles. In contrast, only the spin-1 exchange gives the dominant contribution to the process in the high-energy region, i.e., the contact-term contribution.

(7) Finally, as a single-polarization observable, we compute the photon-beam asymmetry Σ as a function of $\cos\theta$, showing that the nontrivial interference between the contact-term and t-channel contributions plays a dominant role in reproducing the Σ curves.

In conclusion, the present theoretical framework can reproduce the available experimental data qualitatively well, although the resonances and higher-spin meson exchanges,

which are not considered here, might improve the deviations observed in the region $E_\gamma \lesssim (3\text{–}4)\,\mathrm{GeV}$. In particular, it also turns out that the role of the ansatz for the Feynman-Regge interpolation is very crucial in correctly reproducing the experimental data in the higher-energy region. However, being different from the $\Lambda(1520, 3/2^-)$ photoproduction, the t-channel meson exchange and contact-term contributions are competing with each other, especially for the lower-energy region. However, we also note that, although the interpolation plays a significant role in reproducing the data qualitatively, we still have several uncertainties and unknown factors in this highly phenomenological approach: We do not have a firm theoretical ground for it, especially for the ansatz, so that the form of the ansatz has not been uniquely determined yet. Moreover, the interpolation effects can nevertheless be replaced by other Feynman diagrams, such as the nucleon and hyperon resonances, or the production mechanisms, which are not taken into account and tested in the present work of this exploratory study. For more concrete applications of this interpolation approach, those issues mentioned above will be addressed intensively in future works. We expect that the results from the present theoretical work would be a useful guide for the high-energy photon-beam experiment, such as the future experiments planned in LEPS2 at SPring-8 and CLAS12 at Jefferson Laboratory, for instance. More sophisticated works, with other $\pi\Delta$ isospin channels, baryon resonances, and other contributions as mentioned, are in progress and will appear elsewhere.

[1] CLAS Collaboration, K. Hicks, D. Keller, and W. Tang , Nucl. Phys. Proc. Suppl. **210–211**, 115 (2011).

[2] T. Hotta (LEPS Collaboration), Int. J. Mod. Phys. A **26**, 456 (2011).

[3] V. D. Burkert and T. S. H. Lee, Int. J. Mod. Phys. E **13**, 1035 (2004).

[4] S. I. Nam, A. Hosaka, and H.-Ch. Kim, Phys. Rev. D **71**, 114012 (2005).

[5] T. Nakano, talk given at the 11th Asia Pacific Physics Conference (APPC11), Shanghai, China.

[6] H. Toki, C. Garcia-Recio, and J. Nieves, Phys. Rev. D **77**, 034001 (2008).

[7] S. I. Nam, Phys. Rev. C **81**, 015201 (2010).

[8] S. I. Nam and C. W. Kao, Phys. Rev. C **81**, 055206 (2010).

[9] B. G. Yu, T. K. Choi, and W. Kim, Phys. Rev. C **83**, 025208 (2011).

[10] CLAS12, [http://www.jlab.org/Hall-B/clas12/].

[11] LEPS2, [http://www.hadron.jp/].

[12] M. Ripani *et al.*, Nucl. Phys. A **672**, 220 (2000).

[13] J. C. Nacher and E. Oset, Nucl. Phys. A **674**, 205 (2000).

[14] R. B. Clark, Phys. Rev. D **18**, 1444 (1978).

[15] G. R. Goldstein and J. F. Owens, Nucl. Phys. B **71**, 461 (1974).

[16] W. Rarita and J. Schwinger, Phys. Rev. **60**, 61 (1941).

[17] S. Ozaki, H. Nagahiro, and A. Hosaka, Phys. Rev. C **81**, 035206 (2010).

[18] Particle Data Group, K. Nakamura , J. Phys. G **37**, 075021 (2010).

[19] H.-Ch. Kim and M. Praszalowicz, Phys. Lett. B **585**, 99 (2004).

[20] G. S. Yang, H.-Ch. Kim, M. Praszalowicz, and K. Goeke, Phys. Rev. D **70**, 114002 (2004).

[21] M. A. B. Beg, B. W. Lee, and A. Pais, Phys. Rev. Lett. **13**, 514 (1964).

[22] Particle Data Group, C. Amsler *et al.*, Phys. Lett. B **667**, 1 (2008).

[23] J. A. Niskanen, Phys. Lett. B **107**, 344 (1981).

[24] J. Flender and M. F. Gari, Z. Phys. A **343**, 467 (1992).

[25] H. Haberzettl, C. Bennhold, T. Mart, and T. Feuster, Phys. Rev. C **58**, 40 (1998).

[26] R. M. Davidson and R. Workman, Phys. Rev. C **63**, 025210 (2001).

[27] H. Haberzettl, K. Nakayama, and S. Krewald, Phys. Rev. C **74**, 045202 (2006).

[28] T. Regge, Nuovo Cim. **14**, 951 (1959).

[29] M. Vanderhaeghen, M. Guidal, and J. M. Laget, Phys. Rev. C **57**, 1454 (1998).

[30] T. Corthals, J. Ryckebusch, and T. Van Cauteren, Phys. Rev. C **73**, 045207 (2006).

[31] T. Corthals, T. Van Cauteren, J. Ryckebusch, and D. G. Ireland, Phys. Rev. C **75**, 045204 (2007).

[32] J. W. C. McNabb *et al.* (CLAS Collaboration), Phys. Rev. C **69**, 042201 (2004).

[33] A. V. Anisovich *et al.*, Eur. Phys. J. A **34**, 243 (2007).

[34] LAMP2 Group, D. P. Barber *et al.* , Z. Phys. C **7**, 17 (1980).

[35] J. Ballam *et al.*, Phys. Rev. D **5**, 545 (1972).

[36] W. Struczinski *et al.*, Nucl. Phys. B **47**, 436 (1972).

[37] J. Ballam *et al.*, Phys. Rev. D **7**, 3150 (1973).

[38] LAMP2 Group, D. P. Barber *et al.*, Z. Phys. C **6**, 93 (1980).

[39] A. Boyarski *et al.*, Phys. Rev. Lett. **22**, 148 (1969).

[40] R. L. Anderson *et al.*, Phys. Rev. D **14**, 679 (1976).

[41] D. J. Quinn, J. P. Rutherfoord, M. A. Shupe, D. J. Sherden, R. H. Siemann, and C. K. Sinclair, Phys. Rev. D **20**, 1553 (1979).

[42] Aachen-Hamburg-Heidelberg-Munich Collaboration, W. Struczinski *et al.*, Nucl. Phys. B **108**, 45 (1976).

[43] Brown-Harvard-MIT-Padova-Weizmann Institute Bubble Chamber Group, Phys. Rev. **155**, 1468 (1967).

[44] N. Muramatsu *et al.*, Phys. Rev. Lett. **103**, 012001 (2009).

[45] K. Schilling, P. Seyboth, and G. E. Wolf, Nucl. Phys. B **15**, 397 (1970); **18**, 332 (1970).

[46] S. P. Barrow *et al.* (CLAS Collaboration), Phys. Rev. C **64**, 044601 (2001).

[47] W. Roberts and T. Oed, Phys. Rev. C **71**, 055201 (2005).

[48] A. M. Sandorfi, S. Hoblit, H. Kamano, and T. S. Lee, J. Phys. G **38**, 053001 (2011).

[49] See [http://plot.micw.eu/(PLOT)].

[50] See [http://jaxodraw.sourceforge.net/] (JAXODRAW).